J Mater Sci (2015) 50:6041–6049
DOI 10.1007/s10853-015-9151-5

Shear thickening of suspensions of porous silica nanoparticles

Qianyun He[1] · Xinglong Gong[1] · Shouhu Xuan[1] · Wanquan Jiang[2] · Qian Chen[1]

Received: 26 March 2015 / Accepted: 3 June 2015 / Published online: 17 June 2015

Abstract In this work, shear thickening (ST) performance of a novel suspension of porous silica nanoparticles was systematically studied. The porous silica nanoparticles which were synthesized by using CTAB as a pore-forming agent were dispersed into ethylene glycol to form shear thickening fluid (STF). Both the steady and oscillatory shear rheological properties of the STF were characterized. The STF showed distinct ST effects when the concentration of the porous nanoparticles was only 42.5 wt%. This value was much lower than the previously reported STF prepared by non-porous particles. The viscosity increased from 0.80 to 14.3 Pa s by increasing the shear rate from 0.1 to 49.4 s^{-1}, while a noticeable overall downward trend with a high initial viscosity was found in the prepared suspension of non-porous silica. The results indicated that porous nature of the silica nanoparticles could remarkably influence the ST effect. A possible enhancing mechanism was proposed and it was found that the difference of macroscopic rheology behavior was mainly according to interfacial interaction between the porous silica nanoparticles. This work provided valuable information for understanding the relationship between the porous characteristics and ST behavior.

✉ Xinglong Gong
gongxl@ustc.edu.cn

[1] CAS Key Laboratory of Mechanical Behavior and Design of Materials, Department of Modern Mechanics, University of Science and Technology of China (USTC), Hefei 230027, People's Republic of China

[2] Department of Chemistry, USTC, Hefei 230026, People's Republic of China

Introduction

Shear thickening is a kind of non-Newtonian flow behavior, in which the viscosity non-linearly increases with increasing the shear rate [1]. Usually, the densely packed suspensions of nano-sized particles exhibit the typical ST behavior, thus they are defined as the shear thickening fluid (STF). Under the action of an external stress or shear, the fluidic STF becomes a yield material and its physical state transforms to a solid-like state. The process is reversible, which means that the solid-like state will back to fluid-like state again once the applied stress is removed. Because of their effective energy dissipation in response to external stimuli [2, 3], the STFs display significant advantage for use in sports shoe cushioning, damping devices, ballistic protection [4–6], etc.

The potential mechanism for the ST has been intensively studied and the universally accepted one is the hydrocluster theory. It claimed that the short-range hydrodynamic lubrication forces dominated over interparticle forces, thus shear-induced non-equilibrium self-organization particles came into stress-bearing clusters [7]. This view was predicted by Stokesian dynamics simulation [8] and revealed through a series of experiments, such as rheo-optical experiments [9], small angle neutron scattering measurements [7, 10], and stress-jump measurements [11]; and clusters were observed directly by combining fast confocal microscopy with simultaneous force measurements [12]. To fully explore the ST mechanism, much effort has been conducted on studying the parameters that determine the form and extent of ST. Various parameters such as the dispersed particles, medium [1, 13, 14], volume fraction [1, 13], and additives [15–18] were systematically discussed.

Because the distance between hydroclustered particles was considered to be on the order of nanometers,

macroscopic ST behavior directly reflected the microscopic particles' surface structure and the relative short-range forces [19]. It was found that the surface characteristics of dispersed particles significantly affected the rheological properties of the STFs [20, 21]. Chu B et al. reported that the heat treatment could affect the interparticle interactions by changing their surface chemistry, and thus further affect the macroscopic ST behavior of the suspensions [20]. Yu et al. demonstrated a great effect of particles surface treatment on increasing the maximum mass fraction in the STFs [21]. As described above, rheological properties of suspensions were related to the dispersed particles' structure. To further investigate it, inorganic [22] and polymer particles [23] with various shapes such as spheres, rods, plates, and grains [24–26] were employed as the dispersing phase in the STFs. By varying the size [4, 27] and size distribution [4, 28], optimum STFs were obtained.

However, all the referenced STFs were composed of solid particles, few work has been reported on porous particle-based STF. Mesoporous microparticles have drawn increasing attention due to their wide applications in biology, catalysis, separation, etc. In comparison to the solid ones, they exhibited unique advantages such as high surface areas, well-defined pore structures, and tunable pore sizes [29–31]. Due to their low density, the suspensions prepared by porous particles would significantly reduce the total mass at the same volume fraction. This advantage could not only reduce the mass for comfort and portability but also improve economic efficiency for industrial processes, which would enhance their practical applications in flexible protective gear. By dispersing porous particles in polar liquids, the high specific surface areas and roughness surface nature of the porous particles may influence the interfacial interaction between particles and dispersing medium, and then change ST behavior. To this end, the study of porous particle-based concentrated suspensions would not only enable us to achieve high-performance STF, but also help us to deepen the understanding of the ST mechanism.

In this work, the porous silica nanoparticles were synthesized and dispersed into ethylene glycol to prepare STF. The ST performance of the product was evaluated by both the steady shear and oscillatory shear testing. The reversible property and the influence of temperature on the ST performance of the suspensions of porous silica were carefully analyzed for their practical engineering applications. Based on the above results, the possible mechanism for the formation of ST phenomenon of suspensions of porous nanoparticles was proposed. This work provided a novel method for high-performance STF and valuable information to understand the relationship between particles' structure and ST behavior.

Experimental

Materials

Tetraethyl orthosilicate (TEOS, analytical reagent), cetyltrimethyl ammonium bromide (CTAB, analytical reagent), aqueous ammonia solution ($NH_3 \cdot H_2O$, analytical reagent), ethanol (analytical reagent), and ethylene glycol (analytical reagent) were purchased from Sinopharm Chemical Reagent Co., Ltd and used without further purification. The commercial hydrophilic fumed silica nanoparticles were bought from Beijing Aigao Technology Co., Ltd. Doubly distilled water was used throughout the experiment.

Preparation of concentrated suspensions

Firstly, porous silica nanoparticles were synthesized via the combining Stöber-Calcination method. The precursors of the porous silica were obtained by chemical reaction that occurred in a three-neck flask connecting to a mechanical stirrer. The ambient temperature was kept at 40 °C in a water bath during the synthesis. 5 g of CTAB was dissolved in 300 ml of ethanol. Then, 16 ml of ammonia solution and 250 ml of doubly distilled water were added under vigorous stirring at a speed of 800 rpm. 1 h later, 25 ml of TEOS was added dropwise into above mixture. After the reaction lasted for 24 h, the gel-like non-porous silica/CTAB composite nanoparticles product was harvested by centrifugation, washed with ethanol and doubly distilled water, and dried in a vacuum oven at 40 °C. The particles finally obtained were divided into two parts. One part was calcined in air at 550 °C for 5 h to get porous structure, and the other was used as a contrast. The as-prepared porous particles were evenly distributed in ethylene glycol by continuous ball milling for 24 h to obtain the suspension.

The commercial fumed silica nanoparticles were treated under the same conditions. For simplicity, non-porous silica/CTAB composite nanoparticles, porous silica nanoparticles, non-porous fumed silica nanoparticles, and calcined fumed silica nanoparticles were defined as np-SiO_2, p-c-SiO_2, np-fSiO_2, and np-c-fSiO_2, respectively.

Characterization

Morphologies of silica nanoparticles were observed using a Sirion200 scanning electron microscope (SEM). The surface features of nanoparticles were recorded by a JEM-2100F field emission transmission electron microscope (FETEM) with an accelerating voltage of 200 kV. The thermal stability of np-SiO_2 was measured using the thermogravimetric analyzer (DTG-60H). The infrared spectra

were collected in the wavenumber range 4000–400 cm^{-1} with a TENSOR27 Fourier transform infrared (FTIR) spectrometer. The specific surface area and pore volume were taken on a Tristar II3020 M surface area and porosity analyzer by nitrogen sorption at 77 K.

Rheological measurement

All the rheological measurements were carried out on a controlled-stress rheometer (Anton-Paar MCR301). A cone-plate geometry having a cone angle of 0.2° and a diameter of 25 mm was assembled as instrument accessory. Some samples with a high yield stress tended to be solid-like state at rest, which made the stress sensor of the rheometer overloaded when cone-plate geometry contacted them. The viscosity could not be measured properly. So a parallel-plate geometry having a diameter of 20 mm was chosen, and a 1-mm gap size was set during the measurement. Steady shear test and oscillatory shear test were carried out on each sample. The rheometer was programmed to perform a steady pre-shear of 60 s to remove loading effect before each measurement.

Results and discussion

Characterization of the nanoparticles

Morphologies of as-prepared silica particles were observed by SEM. Figure 1a, b shows the SEM images of np-SiO_2 and p-c-SiO_2, respectively. It was found that np-SiO_2 was composed of nearly spherical nanoparticles with an average diameter of 680 nm. Although some irregular particles were presented in the SEM, the surface of the particles was curved, indicating that the particles tended to form spherical particles during the synthesis. Different from the reported monodisperse porous silica nanospheres, the yield of these particles was on gram scale, thus the non-uniform morphology was reasonable. After calcination, the np-SiO_2 transformed to the p-c-SiO_2. Similar size and shape are found in Fig. 1b, indicating that the calcination would not change the outer size and shape of the silica particles, while only led to the porous nature. To further investigate the inner nanostructure of the as-prepared nanoparticles, the high-magnification TEM images of np-SiO_2 and p-c-SiO_2 were presented (Fig. 1c, d). The np-SiO_2 exhibited solid structure and no pores were found. However, after removing the CTAB template, a large amount of pores with size about 2 nm were clearly presented for the p–c-SiO_2 (Fig. 1d). Moreover, these nanopores were arrayed perpendicularly to the particles' surface. To further understand the influence of calcination and porous structure, the commercial fumed silica nanoparticles were also studied. As shown in Fig. 2, the pristine fumed silica nanoparticles were non-porous with a primary size of 12 nm. They fused into aggregates which could not be disrupted by shear [22]. The heating treatment showed few influence on the nanoparticles, and similar morphologies and sizes were obtained after the calcinations.

In this synthesis, the p-c-SiO_2 was obtained by heating the np-SiO_2 to remove the CTAB template. Figure 3 shows the thermogravimetric curve of np-SiO_2, which indicated that the weight of sample decreased with raising temperature. The first weight loss (4.65 %) observed at 100 °C was attributed to water evaporation. When the temperature increased to 200 °C, the weight sharply decreased. The weight loss reached to 31.21 % when the temperature increased to 550 °C. It was reported that the CTAB decomposed at 248–251 °C under normal conditions, and thus, the sharp weight loss was ascribed to the decomposition of the CTAB. Here, these CTAB molecules were confined with the silica matrix, thus the weight loss observed in the range of 550–700 °C was considered to be the CTAB residues.

The FTIR analysis was further employed to track the transformation process of the np-SiO_2 to p-c-SiO_2. Figure 4a, b shows the FTIR spectrum of np-SiO_2 and p-c-SiO_2, respectively. Typically, the absorption bands at 2924, 2853, and 1479 cm^{-1} are clearly observed in Fig. 3a, and they were attributed to the CH_2 and CH_3 groups in CTAB. However, after the heating treatment, these adsorption bands disappeared, indicating the entirely removing of the CTAB molecules. Only the characteristic Si-O-Si absorption was found in the p–c-SiO_2 and np-c-fSiO_2, which demonstrated the as-obtained products were composed of pure silica.

The specific surface area and pore size distribution were calculated from nitrogen BET adsorption/desorption isotherms (Fig. 5). It was found that the specific surface area of p–c-SiO_2 was 794.50 $m^2\ g^{-1}$ which was much higher than the 10.12 $m^2\ g^{-1}$ for np-SiO_2. The higher BET area also indicated the formation of porous nanostructure. A typical type IV isotherm including a hysteresis loop was observed according to the nomenclature by IUPAC for p–c-SiO_2, which confirmed the existence of mesopore surface. At the same time, a type III isotherm which was convex to the P/P_0 axis could be seen for np-SiO_2, corresponding to non-porous nanoparticles [32]. Moreover, the BJH adsorption average pore diameter was calculated to be 3.01 nm for p–c-SiO_2 (inset of Fig. 5), which agreed well with the above analysis.

The rheology behavior of porous silica nanoparticles suspensions

The porous silica nanoparticles were dispersed into ethylene glycol to form the concentrated suspension. Figure 6

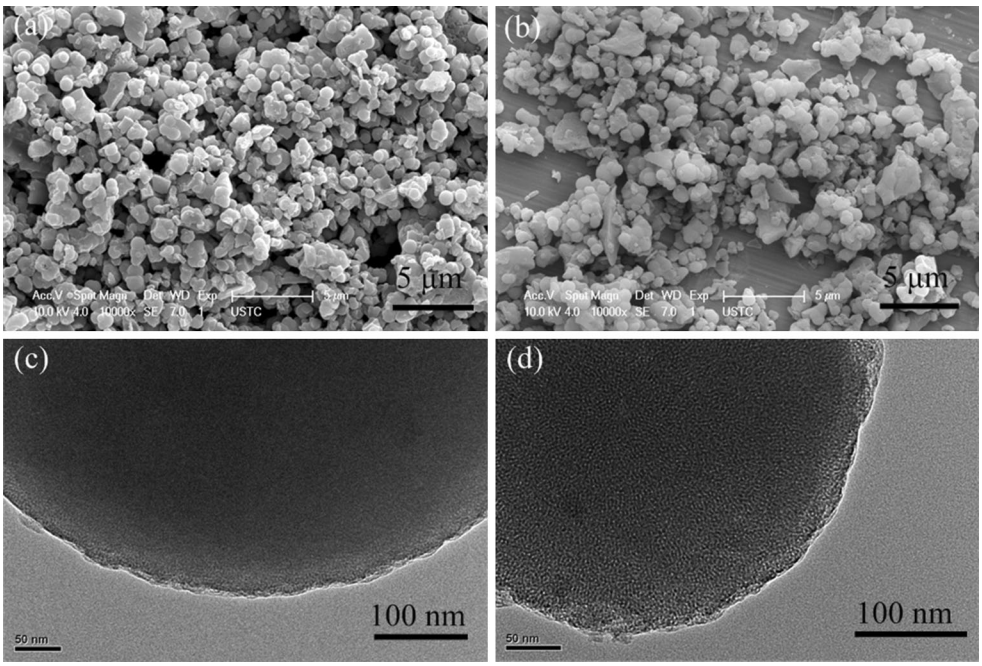

Fig. 1 SEM and TEM images of np-SiO_2 (**a**, **c**) and p-c-SiO_2 (**b**, **d**)

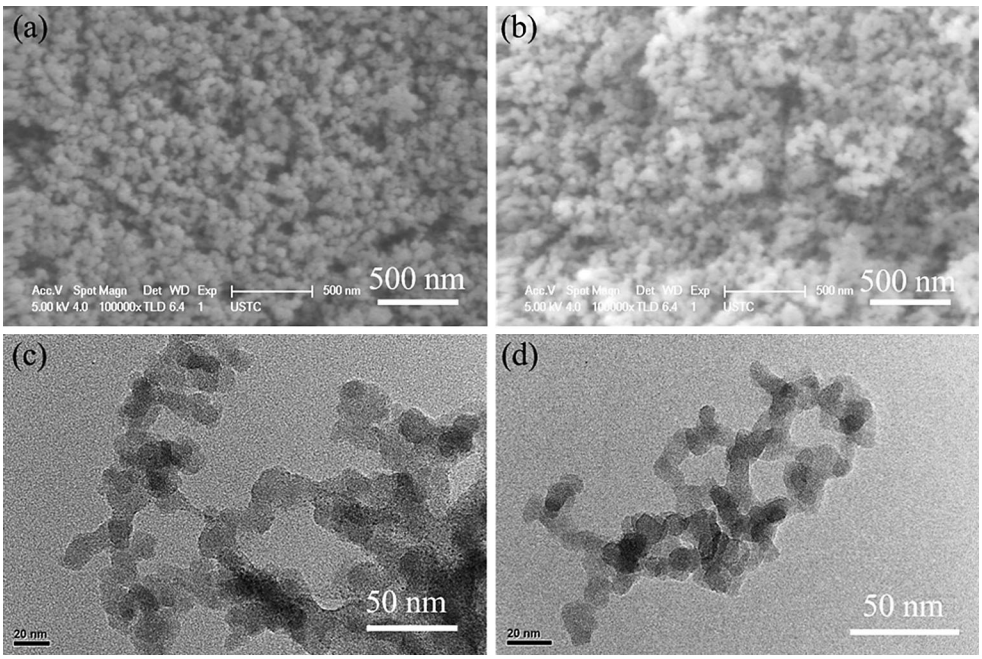

Fig. 2 SEM and TEM images of np-fSiO_2 (**a**, **c**) and np-c-fSiO_2 (**b**, **d**)

shows the shear-rate-dependent viscosity of the p–c-SiO_2-based STF with 42.5 wt%. It could be observed that the suspension of p–c-SiO_2 exhibited shear thinning at low shear rate with initial viscosity of 0.80 Pa·s. Then, as soon as the shear rate increased from 0.1 to 49.4 s^{-1}, the viscosity increased to 14.3 Pa s, which indicated the occurrence of the typical ST phenomenon. Here, the rheological property of the suspension of np-SiO_2 was also investigated. A noticeable overall downward trend was found for the suspension. From the data, we could find that the suspension possessed a high initial viscosity of 1880 Pa s at the shear rate of 0.1 s^{-1}, and it decreased to 3.41 Pa s at the shear rate of 92.1 s^{-1}. From the above analysis, it was clear that p-c-SiO_2 and np-SiO_2 had the similar size, shape,

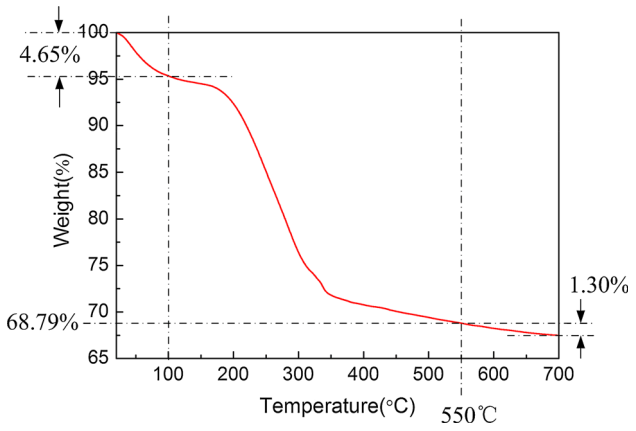

Fig. 3 Thermogravimetric *curve* of np-SiO_2

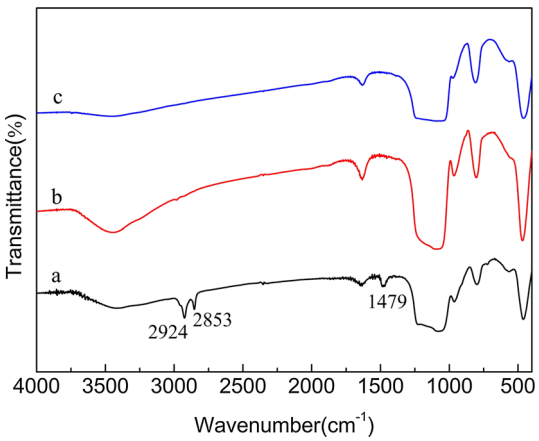

Fig. 4 FTIR spectra of np-SiO_2 (**a**), p-c-SiO_2 (**b**), and np-c-fSiO_2 (**c**)

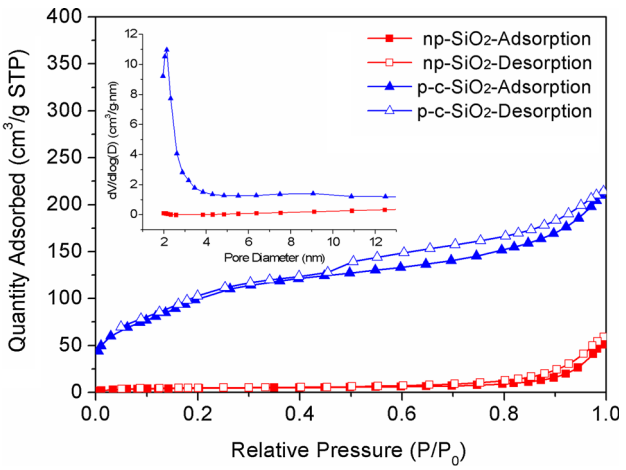

Fig. 5 Nitrogen BET adsorption/desorption isotherm of np-SiO_2 and p-c-SiO_2. *Inset* pore size distribution of np-SiO_2 and p-c-SiO_2

and ingredient. Therefore, the ST must be originated from the porous nanostructure.

To further investigate the effect of calcination, the commercial fumed silica nanoparticles were also employed

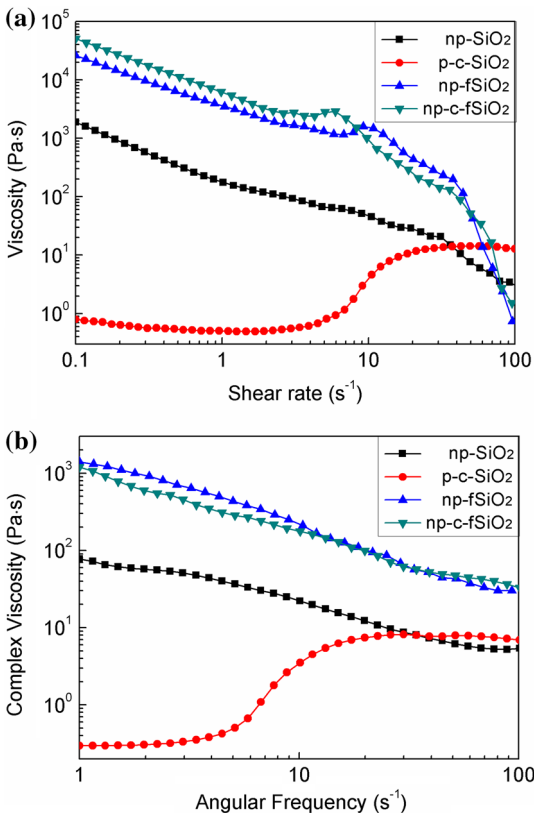

Fig. 6 **a** Viscosity versus shear rate for suspensions of all samples under steady shear. **b** Complex viscosity versus angular frequency for suspensions of all samples under dynamic oscillatory shear. All points were plotted on a log–log scale

as the precursor for preparing the concentration suspensions. Different from our prepared silica particles, the bulk density of the fumed silica was very small. Since ethylene glycol was a polar solvent, the hydrophilic fumed silica could dissolve in the ethylene glycol and the as-prepared suspension was like paste. If the mass fraction was too high, the commercial silica was very difficult to be dispersed into the solvent, because of the high viscosity. Therefore, the mass fraction of the dispersed silica was only 21.0 %. Both the np-fSiO_2 and np-c-fSiO_2 were used to prepare the concentrated suspensions, and Fig. 6 shows their rheological properties. An entire shear thinning could be observed during increasing the shear rate. In the repeated experiments, a slight fluctuation of viscosity sometimes could also be observed. The suspensions of np-fSiO_2 and np-c-fSiO_2 were solid-like state without applying any impact. The initial viscosities of the two samples were on the 10^4 Pa s scale at the shear rate of 0.1 s^{-1}, and their shear-rate-dependent viscosity was similar to the np-SiO_2 under steady shear. The curves for the np-fSiO_2 and np–c-fSiO_2 were almost the same. To this end, we could conclude that the heating treatment was not the dominant factor for the ST.

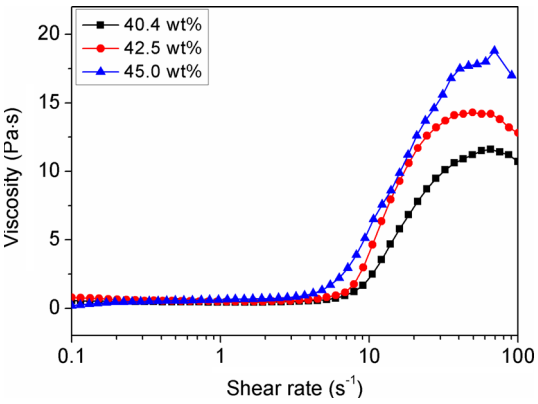

Fig. 7 Viscosity versus shear rate for suspensions of different p–c-SiO_2 mass fractions: 40.4, 42.5, 45.0 % under steady shear

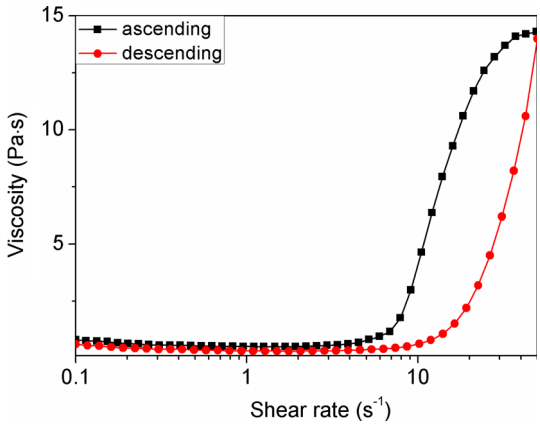

Fig. 8 Reversible property of porous silica nanoparticle-based STF

Actually, the p-c-SiO_2 and np-SiO_2 particles had the similar inner structures except the pores of the np-SiO_2 particles were filled with CTAB molecular templates. After dispersing into the ethylene glycol, the pores of the p-c-SiO_2 could be filled by the solvent which may change the interactions of the particle–solvent and particle–particle. Therefore, the concentrated suspension of p-c-SiO_2 exhibited typical ST effects. Figure 6b shows the rheological properties of all the above suspensions under dynamic oscillatory shear. Similarly, except for the p-c-SiO_2, the other three samples did not show evident ST phenomenon, and agreed well with the above results.

The viscosity versus shear rate curves for suspensions of different p-c-SiO_2 mass fractions are given in Fig. 7. The higher the concentration, the smaller the critical shear rate. Besides, the maximum viscosity increased as the mass fraction of particles increased. The result was consistent with the previous work [13].

Reversible property and temperature stability of the STF based on the porous silica nanoparticles

The STFs should be steady, reversible, and show evident ST effect under external stimuli in a wide temperature range for their practical engineering applications. So the reversible property and temperature stability of the as-synthesized suspensions of porous silica were also investigated in this work.

The viscosity of the suspension of porous silica at 42.5 wt% was measured for both ascending and descending steady shear rate sweeps (Fig. 8). At the beginning, the viscosity was almost kept a constant with a slight decrement. When the shear rate reached to a critical point, the viscosity quickly increased with the shear rate, indicating the presence of the ST. As soon as the shear rate decreased, the viscosity immediately decreased. Although the viscosities in the descending curve were smaller than in the ascending curve, it was noted that they had the similar tendency. The flow curve showed weak hysteresis at high shear rate, which could be explained by the effect of gravity of nanoparticles. The as-prepared porous nanoparticles aggregated in some degree (Fig. 1b), which was equivalent to improve the average particle size, enhance the effect of gravity, and promote the dissolution rate of hydroclusters. If the dispersion nanoparticles were uniform, the two curves would tend to be overlapped. Therefore, the differentiation of the descending curve and ascending curve could be ascribed to the unstable hydroclusters in the absence of external force. With decreasing of shear rate, the formed hydroclusters would be dissolved and dispersed in the solvent again. To this end, uniform porous silica-based STF would be the key point of our future research.

Figure 9a shows the rheology behavior of the STF at 42.5 wt% by varying the temperature from 5 to 40 °C. With increasing the temperature, the viscosity entirely slightly decreased. The STF kept the ST effect very well even the temperature increased to 40 °C, indicating the product was very stable which would benefit their further practical applications. With increasing the temperature, the initial viscosity and the maximum viscosity in ST region decreased, while the critical shear rate increased. For example, the maximum viscosity was 22.8 Pa s at 5 °C and 4.69 Pa s at 40 °C, and the initial viscosity was 1.02 and 0.256 Pa s, respectively.

In terms of the hydrocluster mechanism, ST was usually weakened by increasing temperature. According to theory of Brownian motion, by rising temperature, molecules of dispersing medium moved heavily accompanied by the faster dispersed nanoparticles migration. Therefore, the Brownian motion resulted in nanoparticles keeping away from each other. When suffered an external stress or shear, the force balance broke, hydrodynamic force dominated over the interaction force between particles, and the ST behavior occurred. At higher temperature, it would be more

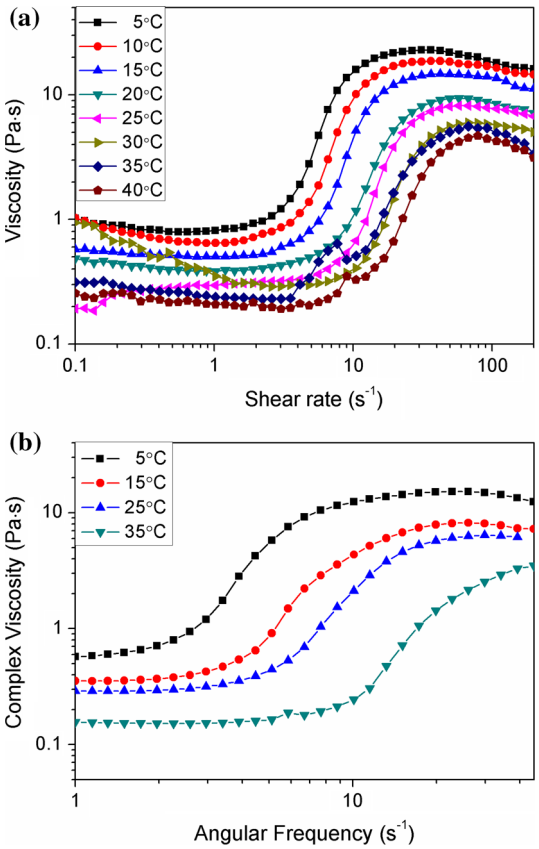

Fig. 9 Viscosity versus shear rate for suspensions of p-c-SiO_2 under steady shear (**a**), and complex viscosity versus angular frequency for suspensions of p-c-SiO_2 under dynamic oscillatory shear ($\gamma = 200$ %, **b**) showing the evolution with increasing temperature

difficult for the hydrodynamic force to force particles to get close to form hydroclusters. In this case, stronger applied force was needed, thus the critical shear rate increased and the maximum viscosity decreased. Figure 9b shows the complex viscosity vs. angular frequency for the STF at 5, 15, 25, and 35 °C. The dynamic oscillatory sweep curves were resembled to the trend of the steady shear sweep curves.

The ST effect mechanism of the suspensions of porous silica nanoparticles

Based on the above results, it was found that the suspensions of porous silica nanoparticles exhibited more distinct ST behavior than non-porous nanoparticles. According to the above analysis, the origination of the ST effect maybe came from the difference of the microstructure. The surface characteristics dominated the microscopic interfacial interaction while further determined the ST behavior. In this work, a possible mechanism for rheology behavior of both suspensions was proposed, as shown in Fig. 10.

The interfacial interaction between dispersed nanoparticles and disperse medium was an important factor for ST effects. George Batchelor' articles indicated that force was transmitted between adjacent particles through squeezing intervening fluid resulting in a disturbed local flow field [33]. The dominated hydrodynamic forces originated from hydrodynamic pressure between nanoparticles [19], which related to interfacial interaction between nanoparticles and solvent. For silica nanoparticles, large amounts of silicon–oxygen bond and silanol bond existing inside and outside of the nanoparticles determined their surface chemical properties. In the STF, the silica nanoparticles separated from each other by solvent ethylene glycol whose molecule diameter was on the scale of 10^{-9} m. For the porous silica, there are large numbers of mesopores with size about 3.0 nm in the particles' surface, which greatly increased particles' BET specific surface area. Thus, more solvent molecules could fully contact with porous nanoparticles near solid–liquid interface than the non-porous ones. Ethylene glycol was polar and they preferentially formed hydrogen bonds with the silanol groups on nanoparticles' surface [20]. So the ethylene glycol was believed to be adsorbed both in the pores and on the surface of nanoparticles, in Raghavan's opinion, forming a solvation layer [34]. The solvation layer led to short-range repulsions to stabilize the monodisperse particles. Contrastively, for the non-porous silica, particles contacted insufficiently with solvent for a low specific surface area, especially some CTAB exposed in the surface occupied space. The limited hydrogen bonding between solvent molecules and particles gave way to interact directly between particles [34]. Then, the particles connected and the system was unstable. Macroscopically, a noticeable shear thinning with a high initial viscosity is observed in Fig. 6.

We considered that the different rheological behavior of the suspensions was due to the change in the solvation layer of the particles. A denser solvation layer indicating stronger repulsive force may cause the enhancement of the ST effect in suspensions [20]. Porous structure contributed to strengthen the connection between particles and solvent. The widespread contact of the nanoparticles and the solvent facilitated the formation of denser solvation layer and the hydroclusters produced by hydrodynamic lubrication forces when subjected to shear rate.

Conclusions

In this work, a novel suspension of porous silica nanoparticles was prepared and its ST behavior was studied. It was found that various affecting factors, such as the structure of the dispersing nanoparticles exhibited typical influence on its rheological properties. With the increase of

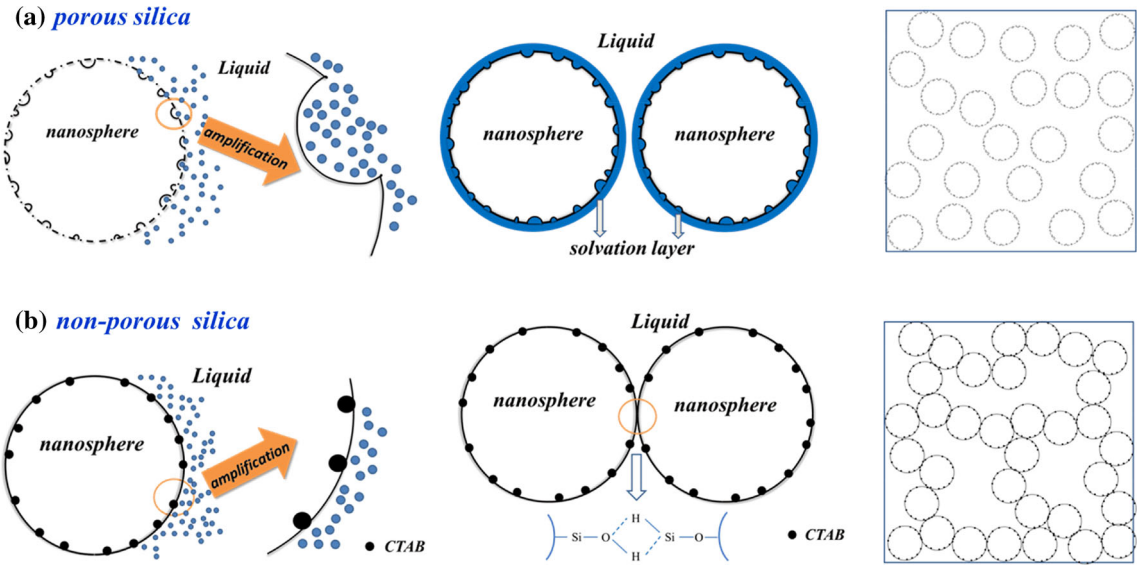

Fig. 10 The microcosmic mechanism of suspensions of porous and non-porous silica nanoparticles

shear rate, the viscosity of the STF increased from initial viscosity of 0.80 Pa s to the maximum viscosity of 14.3 Pa s at the shear rate of 49.4 s^{-1}. Compared to the behavior of suspensions of non-porous silica nanoparticles, it was found that porous nature in dispersed nanoparticles could remarkably influence the ST effect. The STF showed distinct ST effects even the concentration of the porous nanoparticles was only 42.5 wt%. This value was much lower than the previously reported STF prepared by non-porous particles. The reversible property and the influence of temperature on the ST performance of the suspensions of porous silica were also investigated for their practical engineering applications. Since the porous nature of the silica nanoparticles, its BET area reached to as high as 794.50 m^2 g^{-1}. The more solvent molecules could fully contact with porous nanoparticles near solid–liquid interface. The possible mechanism based on interfacial interaction was proposed. Finally, this work provided valuable information for understanding the relationship between the porous characteristics and ST behavior.

Acknowledgements This work was supported by Collaborative Innovation Center of Suzhou Nano Science and Technology. Financial supports from the National Natural Science Foundation of China (Grant Nos. 11372301, 11125210) and the National Basic Research Program of China (973 Program, Grant No.2012CB937500) are gratefully acknowledged.

References

1. Brown E, Jaeger HM (2014) Shear thickening in concentrated suspensions: phenomenology, mechanisms and relations to jamming. Rep Prog Phys 77(4):046602
2. Jiang W, Gong X, Xuan S et al (2013) Stress pulse attenuation in shear thickening fluid. Appl Phys Lett 102(10):101901
3. Lee YS, Wagner NJ (2003) Dynamic properties of shear thickening colloidal suspensions. Rheol Acta 42(3):199–208
4. Barnes HA (1989) Shear-thickening ("dilatancy") in suspensions of nonaggregating solid particles dispersed in newtonian liquids. J Rheol 33(2):329–366
5. Zhang XZ, Li WH, Gong XL (2008) The rheology of shear thickening fluid (STF) and the dynamic performance of an STF-filled damper. Smart Mater Struct 17(3):035027
6. Lee YS, Wetzel ED, Wagner NJ (2003) The ballistic impact characteristics of Kevlar® woven fabrics impregnated with a colloidal shear thickening fluid. J Mater Sci 38(13):2825–2833. doi:10.1023/A:1024424200221
7. Maranzano BJ, Wagner NJ (2002) Flow-small angle neutron scattering measurements of colloidal dispersion microstructure evolution through the shear thickening transition. J Chem Phys 117(22):10291–10302
8. Bossis G, Brady JF (1989) The rheology of Brownian suspensions. J Chem Phys 91(3):1866–1874
9. Bender JW, Wagner NJ (1995) Optical measurement of the contributions of colloidal forces to the rheology of concentrated suspensions. J Colloid Interface Sci 172(1):171–184
10. Laun HM, Bung R, Hess S et al (1992) Rheological and small angle neutron scattering investigation of shear-induced particle structures of concentrated polymer dispersions submitted to plane Poiseuille and Couette flowa). J Rheol 36(4):743–787
11. O'Brie VT, Mackay ME (2000) Stress components and shear thickening of concentrated hard sphere suspensions. Langmuir 16(21):7931–7938
12. Cheng X, McCoy JH, Israelachvili JN et al (2011) Imaging the microscopic structure of shear thinning and thickening colloidal suspensions. Science 333(6047):1276–1279
13. Jiang W, Sun Y, Xu Y et al (2010) Shear-thickening behavior of polymethylmethacrylate particles suspensions in glycerine–water mixtures. Rheol Acta 49(11–12):1157–1163
14. Shenoy SS, Wagner NJ (2005) Influence of medium viscosity and adsorbed polymer on the reversible shear thickening transition in concentrated colloidal dispersions. Rheol Acta 44(4):360–371

15. Kamibayashi M, Ogura H, Otsubo Y (2008) Shear-thickening flow of nanoparticle suspensions flocculated by polymer bridging. J Colloid Interface Sci 321(2):294–301
16. Xu Y, Gong X, Peng C et al (2010) Shear thickening fluids based on additives with different concentrations and molecular chain lengths. Chin J Chem Phys 23(3):342–346
17. Franks GV, Zhou Z, Duin NJ et al (2000) Effect of interparticle forces on shear thickening of oxide suspensions. J Rheol 44(4):759–779
18. Ye F, Zhu W, Jiang W et al (2013) Influence of surfactants on shear-thickening behavior in concentrated polymer dispersions. J Nanopart Res 15(12):1–9
19. Wagner NJ, Brady JF (2009) Shear thickening in colloidal dispersions. Phys Today 62(10):27–32
20. Chu B, Brady AT, Mannhalter BD et al (2014) Effect of silica particle surface chemistry on the shear thickening behaviour of concentrated colloidal suspensions. J Phys D-Appl Phys 47(33):335302
21. Yu K, Cao H, Qian K et al (2012) Shear-thickening behavior of modified silica nanoparticles in polyethylene glycol. J Nanopart Res 14(3):1–9
22. Raghavan SR, Khan SA (1997) Shear-thickening response of fumed silica suspensions under steady and oscillatory shear. J Colloid Interface Sci 185(1):57–67
23. Chang L, Friedrich K, Schlarb AK et al (2011) Shear-thickening behaviour of concentrated polymer dispersions under steady and oscillatory shear. J Mater Sci 46(2):339–346. doi:10.1007/s10853-010-4817-5
24. Clarke B (1967) Rheology of coarse settling suspensions. Trans Inst Chem Eng 45(6):251–256
25. Egres RG, Wagner NJ (2005) The rheology and microstructure of acicular precipitated calcium carbonate colloidal suspensions through the shear thickening transition. J Rheol 49(3):719–746
26. Brown E, Zhang H, Forman NA et al (2011) Shear thickening and jamming in densely packed suspensions of different particle shapes. Phys Rev E 84(3):031408
27. Maranzano BJ, Wagner NJ (2001) The effects of particle size on reversible shear thickening of concentrated colloidal dispersions. J Chem Phys 114(23):10514–10527
28. Yang HG, Li CZ, Gu HC et al (2001) Rheological behavior of titanium dioxide suspensions. J Colloid Interface Sci 236(1):96–103
29. Chen H, He J, Tang H et al (2008) Porous silica nanocapsules and nanospheres: dynamic self-assembly synthesis and application in controlled release. Chem Mat 20(18):5894–5900
30. Hoffmann F, Cornelius M, Morell J et al (2006) Silica-based mesoporous organic–inorganic hybrid materials. Angew Chem Int Edit 45(20):3216–3251
31. Tao Y, Kanoh H, Abrams L et al (2006) Mesopore-modified zeolites: preparation, characterization, and applications. Chem Rev 106(3):896–910
32. Sing KSW (1985) Reporting physisorption data for gas/solid systems with special reference to the determination of surface area and porosity (Recommendations 1984). Pure Appl Chem 57(4):603–619
33. Russel WB, Saville DA, Schowalter WR (1989) Colloidal dispersions. Cambridge University Press, New York
34. Raghavan SR, Walls HJ, Khan SA (2000) Rheology of silica dispersions in organic liquids: new evidence for solvation forces dictated by hydrogen bonding. Langmuir 16(21):7920–7930